3D Pressure Field in Lipid Membranes and Membrane-Protein Complexes

O. H. Samuli Ollila,[1] H. Jelger Risselada,[2] Martti Louhivuori,[2] Erik Lindahl,[3] Ilpo Vattulainen,[1,4,5] and Siewert J. Marrink[2]

[1]*Department of Physics, Tampere University of Technology, P.O. Box 692, FI–33101 Tampere, Finland*
[2]*Department of Biophysical Chemistry, University of Groningen, Nijenborgh 4, 9747 AG Groningen, The Netherlands*
[3]*Department of Biochemistry and Biophysics, Stockholm University, SE-10691, Sweden*
[4]*Department of Applied Physics, Helsinki University of Technology, P.O. Box 1100, FI–02015 HUT, Finland*
[5]*MEMPHYS–Center for Biomembrane Physics, Physics Department, University of Southern Denmark, Campusvej 55, DK-5230 Odense M, Denmark*

(Received 19 September 2008; published 19 February 2009)

We calculate full 3D pressure fields for inhomogeneous nanoscale systems using molecular dynamics simulation data. The fields represent systems with increasing level of complexity, ranging from semivesicles and vesicles to membranes characterized by coexistence of two phases, including also a protein-membrane complex. We show that the 3D pressure field is distinctly different for curved and planar bilayers, the pressure field depends strongly on the phase of the membrane, and that an integral protein modulates the tension and elastic properties of the membrane.

DOI: 10.1103/PhysRevLett.102.078101 PACS numbers: 87.16.D−, 87.16.A−, 87.15.A−

Introduction.—The lateral pressure profile, or stress profile, across a cell membrane results from the inhomogeneous nature of the interactions within a membrane. As water, head groups, and acyl chains contribute through different forces, one finds the emergence of a nonuniform pressure profile inside a lipid bilayer. The profile has been proposed to be coupled to membrane-protein structure and functionality in a manner where changes in the pressure profile affect protein activation [1,2] and/or association [3]. The moments of the pressure profile can be connected, e.g., to the mean and Gaussian bending elasticity [4].

While experimental studies of lateral pressure profiles are rare and indirect [5,6], several computational studies have shed light on pressure profiles of planar lipid bilayers [7–10]. In these studies, a bilayer is divided into slabs perpendicular to the membrane normal, and pressure is calculated in each slab. However, this approach does not work for vesicles, membranes with proteins, or heterogeneous bilayers, because in these physiologically relevant cases the pressure profile can not be characterized by the normal coordinate as in a planar bilayer; there is a 3D field instead of a profile. Yet it has been shown that the work exerted by the pressure profile when a protein conformational change takes place is significant, of the order of $10k_BT$ [11,12], and that the lateral pressure profile averaged over the whole membrane is modified by the inclusion of a membrane protein [13]. Indeed, understanding the full 3D coupling for stress arising from protein-lipid interactions is of profound importance and calls for elucidation.

Here, we calculate the full 3D pressure field for a number of systems with varying degree of complexity using molecular dynamics simulations. We define the 3D pressure tensor and derive expressions for planar and spherical symmetry. We apply the new methodology to three cases: lipid vesicles, a membrane with an embedded protein, and a bilayer with liquid-gel phase coexistence. The membrane embedded protein, MscL, is of particular interest as it is mechanosensitive, i.e., it gates in response to membrane tension [14,15].

Theoretical background.—The pressure for an inhomogenous system is represented as a tensor $\mathbf{P}(\mathbf{r})$ that depends on the location $\mathbf{r}$. For a system consisting of pointwise particles with n-body potentials U^n the local pressure can be defined as a sum of kinetic and configurational contribution [8,10,16,17]:

$$p^{\alpha\beta}(\mathbf{r}) = \sum_i m_i v_i^\alpha v_i^\beta \delta(\mathbf{r}-\mathbf{r}_i) - \sum_n \frac{1}{n} \sum_{\langle j\rangle} \sum_{\langle k,l\rangle} (\nabla_{j_k}^\alpha U^n - \nabla_{j_l}^\alpha U^n) \oint_{C_{j_l j_k}} dl^\beta \delta(\mathbf{r}-\boldsymbol{l}), \tag{1}$$

where $C_{j_l j_k}$ is a contour from the particle j_l to the particle j_k, $\langle j\rangle$ stands for summation over all n clusters in the system, $\langle k, l\rangle$ describes summation over all pairs of particles within a given n cluster, and m_i, v_i, and $\mathbf{r}_i$ refer to the mass, velocity, and location of atom i, respectively, and α and β refer to the components. Equation (1) gives a continuous pressure field. To find the pressure tensor $\mathbf{P}_V$ for a volume element V, we have to take an average over the volume element $\mathbf{P}_V = \int_V \mathbf{P}(\mathbf{r}) d\mathbf{r}/V$. Together with Eq. (1) one finds the pressure tensor for volume V

$$p_V^{\alpha\beta} = \frac{1}{V} \sum_{i\in V} m_i v_i^\alpha v_i^\beta + \sum_n \frac{1}{nV} \sum_{\langle j\rangle} \sum_{\langle k,l\rangle} (\nabla_{j_k}^\alpha U^n - \nabla_{j_l}^\alpha U^n) \frac{r_{j_l j_k}^\beta}{N} \times \sum_{\lambda=0}^{N} f_V(\mathbf{r}_{j_l} + \frac{\lambda}{N}\mathbf{r}_{j_l j_k}), \tag{2}$$

where $f_V(\mathbf{r}) = 1$, if $\mathbf{r} \in V$, and zero otherwise. Each vec-

tor $\mathbf{r}_{j_l j_k} = \mathbf{r}_{j_k} - \mathbf{r}_{j_l}$ is divided into N parts and the contribution of a given part λ is added only if the contour goes through V, i.e., if $f_V = 1$. For the contour we use the Irving-Kirkwood (IK) contour [18], see the supplementary material (SM) [19]. We call $\mathbf{P}_V(\mathbf{r})$ as pressure field.

For a system with planar symmetry the local pressure can be divided into planar p_L and normal components p_{zz} via $\mathbf{P}(z) = (\mathbf{e_x e_x} + \mathbf{e_y e_y})p_L(z) + \mathbf{e_z e_z} p_{zz}(z)$, where the coordinate z is along the membrane normal. It follows from planar symmetry that $p_L(z) = p_{xx}(z) = p_{yy}(z)$ depends only on z. Furthermore, the surface tension of a layer between z_1 and z_2 is given by [20] $\gamma = -\int_{z_1}^{z_2} dz \pi(z)$. Traditionally, the integrand of this equation $\pi(z) = p_L(z) - p_{zz}(z)$ is referred to as the lateral pressure profile. The first moment of $\pi(z)$ gives an example of a connection to elastic properties of a layer between z_1 and z_2 [4] via $c_0\kappa = \int_{z_1}^{z_2} dz(z - z_0)\pi(z)$, where c_0 denotes the spontaneous curvature with respect to a pivotal plane z_0, and κ the bending modulus.

For a system with spherical symmetry, e.g., a vesicle, we divide the pressure tensor into tangential p_T and radial p_{rr} components $\mathbf{P}(\mathbf{r}) = (\mathbf{e}_\theta \mathbf{e}_\theta + \mathbf{e}_\phi \mathbf{e}_\phi)p_T(r) + \mathbf{e_r e_r} p_{rr}(r)$, where r is the distance from the origin of the coordinate system. From spherical symmetry, it follows that $p_T(r) = p_{\theta\theta}(r) = p_{\phi\phi}(r)$ depend only on r. A spherical surface with radius R has a surface tension [20]

$$\sigma = -(1/R^2) \int_0^\infty dr r^2 [p_T(r) - p_{rr}(r)]. \qquad (3)$$

The pressure tensor for a system with cylindrical or approximately cylindrical symmetry, e.g., a membrane protein, is discussed in the SM [19]. The pressure tensor becomes diagonal when the coordinate system aligns with the physical surface.

Implementation.—We discretize Eq. (1) into cubes, typically with a linear dimension of 0.1–0.4 nm, allowing us to calculate the average pressure over arbitrary volume elements. The local pressure tensor is calculated for each cube using Eq. (2). The vector between two particles is divided into $N = 100$ segments in Eq. (2). Though increasing N increases computational cost, the segments must be smaller than the cube size.

For a system with spherical symmetry, the pressure tensor is transformed in each cube from Cartesian coordinates $\mathbf{P}(x, y, z)$ to spherical ones $\mathbf{P}'(r, \theta, \phi)$ by applying a transformation matrix $\mathbf{T}$, i.e., $\mathbf{P}' = \mathbf{T}\mathbf{P}\mathbf{T}^T$ [21]. The average of the pressure tensor is calculated over spherical shells $\mathbf{P}'(r) = \langle \mathbf{P}'(r, \theta, \phi) \rangle_{\theta,\phi}$ to get $p_T(r)$ and $p_{rr}(r)$. A similar approach for cylindrical symmetry is described in the SM [19]. Here we refer to these averages as pressure profiles.

For the sake of validation, we also determined the pressure profile in a vesicular system using a novel mean-field boundary potential method [22]. The advantage of this method is the freedom from ambiguity in the virial definition, Eq. (1). See the SM for details [19].

Simulated systems.—The GROMACS package [23] was used for simulations. The coarse grained (CG) MARTINI force field and attached simulation protocol [24–26] were used to model the systems. The temperature was set to 323 K except in the phase coexistence simulation it was 273 K. Time scales are given in CG units. In addition to a DPPC semivesicle, we studied a spherical DOPC vesicle with different amounts of water inside to create two systems with different internal pressures. A tension-free planar DOPC bilayer was modeled for comparison. Further, we modeled a two-phase DPPC bilayer at a constant area per lipid of 0.52 nm^2. The constant area creates a surface tension of 69 mN/m and forces the membrane into a gel-liquid phase coexistence. Finally, a mechanosensitive channel Tb-MscL (PDB: 2oar) was simulated in a DOPC bilayer following [15]. A tension of 39 mN/m was applied to keep MscL in the open state. More details are in [19].

Results.—We first compare the results obtained with the new method to the results obtained independently with the mean-field boundary approach. The comparison is made for a semivesicle adsorbed on a boundary plane. Figure 1 depicts the tangential component $p_T(r)$ for the semivesicle as a function of r calculated using both methods. We see that the virial, Eq. (2), together with the IK contour gives similar results as the force per area calculated from the boundary. In the virial calculation the semivesicle is assumed to be spherically symmetric. This is not exactly true in our case, which leads to the small deviations between the two cases. The results justify the use of the IK contour to calculate local virials in three dimensions.

Because of its curved geometry, a vesicular membrane has distinct properties compared to a lamellar membrane, most noticeable with small radius of curvature. The effect of curvature on the pressure profile across the membrane has not been addressed before. The 3D virial decomposition method allows such an analysis. In Fig. 2(a) the results of this analysis, assuming spherical symmetry for the vesicle, are shown. The pressure is set to zero outside the vesicle, yielding the pressure difference $\Delta\mathbf{P} = \mathbf{P}(r) - \mathbf{P}_{\text{out}}$. The pressure profile for a planar, tensionless DOPC

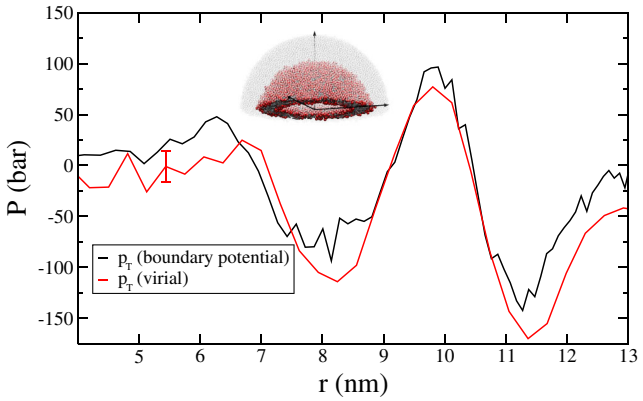

FIG. 1 (color online). The $p_T(r)$ for the DPPC semivesicle as a function of r calculated using mean-field and virial methods.

bilayer is shown for comparison, shifted horizontally such that the negative peaks of the inner monolayer coincide. Most striking differences are the magnitudes of the peaks and the asymmetry in the pressure profile of a vesicle. The asymmetry results from different packing properties [27]: in the inner monolayer the headgroup peak is more pronounced due to the negative curvature and tighter packing of the headgroups, and *vice versa* for the outer monolayer. The broader peaks reflect a less clear boundary between hydrophilic and hydrophobic regions in a vesicle. The results highlight the role of curvature and imply that the pressure profile, and the associated elastic behavior are distinctly different for small vesicles compared to large unilamellar liposomes.

Pressure profiles between vesicles with different internal pressures are compared in Fig. 2(b). The pressure difference is obvious from different bulk values inside the vesicles. Furthermore, the increasing pressure inside a vesicle increases the vesicle size and induces tension into the bilayer quantified by Eq. (3). We approximate the limits of σ considering a minimal and maximal radius R given by the intersections of water and hydrocarbon densities for each monolayer (see Fig. 2). We find $\sigma \approx -(1\text{–}6)$ mN/m and $\sigma \approx (45\text{–}91)$ mN/m for the smaller and larger vesicle, respectively. Comparing these tensions to the experimentally determined gating tension of MscL [28] that is $\sim(10\text{–}20)$ mN/m suggests that if incorporated into these vesicles, the channel would be closed in the smaller one and open in the swollen one.

Next, we analyze the stress profile of a DOPC bilayer with an open MscL channel embedded. We assume cylindrical symmetry and take the average over angles, see the SM [19]. Figure 3(a) presents $\pi(z, r)$ as a function of z (normal coordinate of the bilayer) and r (distance from the center of MscL in cylindrical coordinates). Figure 3(b) shows the surface tension γ for the monolayers and the bilayer. The total tension of the system is (38 ± 1) mN/m as set by the barostat to keep the MscL channel in an open state. However, the tension varies strongly with the lateral position. In the protein region ($r < 4$ nm) the average tension is 33 ± 1 mN/m whereas in the bilayer region ($r > 4$ nm) it is 43 ± 1. This perturbing effect of the protein is maintained across the entire membrane patch. A slowly decaying stress field around the protein is not observed.

Another conclusion drawn from Fig. 3(b) is that the monolayers behave differently. The average tensions for the lower and upper leaflets, protein region included, are (14 ± 1) mN/m and (23 ± 1) mN/m, respectively. The higher tension in the upper leaflet implies that it tends to decrease the area more than the lower one. As a consequence, emergence of spontaneous curvature in the bilayer is anticipated. To quantify this, we calculate the first moment of the pressure profile, see Fig. 3(c). The average over the bilayer region ($r > 4$ nm) gives $\kappa c_0 = (-43 \pm 6) \times 10^{-13}$ J/m for the bilayer, while the average over the whole system yields $\kappa c_0 = (-151 \pm 6) \times 10^{-13}$ J/m. Experimental values for κ for different lipid bilayers vary between $(0.1 - 6) \times 10^{-19}$ J [29]. The effect of an embedded protein on κ is unknown, but a recent simulation study suggests that the area compressibility modulus is

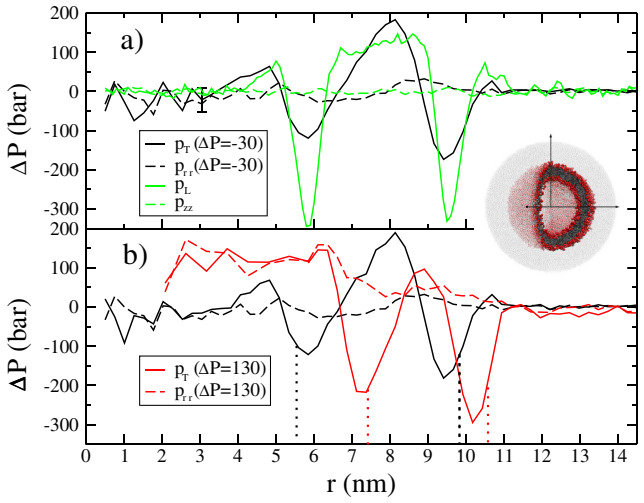

FIG. 2 (color online). Pressure profiles for DOPC bilayers and vesicles. (a) For the bilayer, the solid line and dashed green line stand for p_L and p_{zz}, respectively. For the vesicle, the solid line and dashed black line correspond to p_T and p_{rr} with $\Delta P \approx -30$ bar, in respective order. (b) Results for the vesicle with $\Delta P \approx 130$ bar. Solid line and dashed red line correspond to p_T and p_{rr}, respectively. Black lines are as in panel (a). Vertical dotted lines show the location of intersections between acyl chain and water density.

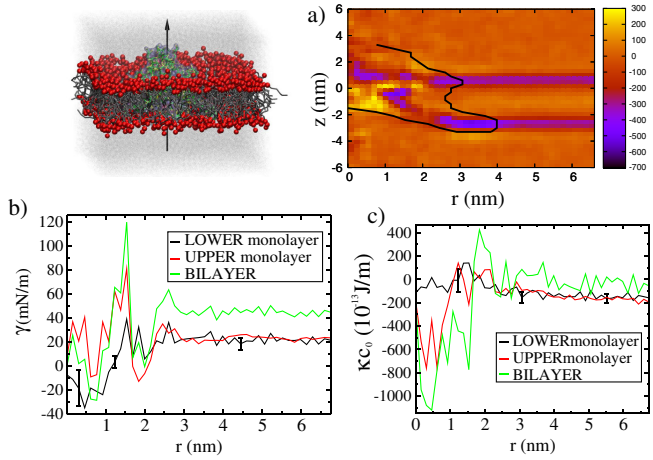

FIG. 3 (color online). Pressure profile of a membrane-protein system. (a) Horizontal axis is the distance from protein center, vertical axis is the normal component of the bilayer (protein center at $z = 0$). The lower and upper leaflets are characterized by $z \in [-4, -1)$ nm and $z \in [-1, 2]$ nm, respectively, and color represents the local pressure (in units of bar). The approximate boundary of the protein region is presented with a full black line (see the SM [19]). (b) Surface tension γ as a function of distance from the protein center r. (c) Product κc_0 vs r. Pivotal planes are located in $z_0 = -2$ nm and $z_0 = 0$ nm, for lower and upper [see order in panel (a) leaflets], respectively.

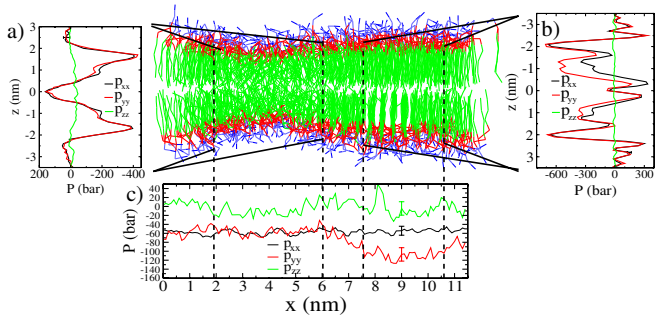

FIG. 4 (color online). Pressure tensor components in (a) liquid and (b) gel phases. (c) Pressure as a function of normal to the phase boundary $\mathbf{P}(x)$ (see text). The pure liquid phase is located between $x = 2$–6 nm and the pure gel between 7.5–10.5 nm.

increased 22% due to inclusion of MscL [30]. Similar behavior can be expected for κ. Using experimental values for κ, we approximate spontaneous curvatures for the whole system and the bilayer region, $c_0 = (-0.025) - (-1.5)\ (\mathrm{nm})^{-1}$ and $c_0 = (-0.0072) - (-0.43)\ (\mathrm{nm})^{-1}$, respectively.

Taken together, our results suggest that inclusion of MscL in a symmetric bilayer causes additional stress in the membrane and introduces a significant spontaneous curvature. In real membranes the spontaneous curvature would either lead to a curved membrane surface, and/or redistribution of lipids between the two leaflets. Here, these are not observed since the time scale of lipid flips-flops is inaccessible and the periodic boundary conditions prevent curving of the membrane.

Finally, we consider a DPPC bilayer in a state of gel-liquid phase coexistence, serving as an example for phase separated membranes. Figure 4 illustrates the liquid and gel domains separated by a $\sim$1.5 nm thick transition region. The lateral pressure profiles are shown in Figs. 4(a) and 4(b), for the liquid and gel phase, respectively. Planar symmetry is assumed for the gel and liquid parts separately. The pressure profile for the liquid phase is similar to that of a homogeneous fluid bilayer as shown in Fig. 2(a). In contrast, in the gel phase it is strikingly different, and is closely reminiscent of the profiles found for bilayers with large amounts of cholesterol [11]. Clearly, the pronounced ordering of the acyl chains in a bilayer gives rise to the complex peaked structure of the pressure profile, complemented by its anisotropic nature in the gel phase.

The pressure field averaged over y and z coordinates $\mathbf{P}(x) = \langle \mathbf{P}(x, y, z) \rangle_{yz}$ is presented in Fig. 4(c). Both lateral components are negative, as the bilayer is under stress, inducing gel-liquid coexistence. Whereas $p_{xx}(x)$ and $p_{zz}(x)$ are basically constant, $p_{yy}(x)$ is smaller in the gel than in the liquid phase. This is due to the phase boundary lying along the y direction, with an associated line tension.

Concluding remarks.—We have shown the prominent role of 3D stress profiles inside membranes and membrane-protein complexes. The pressure field is distinctly nonuniform both across the membranes and also in the membrane plane. This is most evident at interfaces that bridge membrane domains in different phases, and in membranes rich in proteins where the pressure field and the resulting membrane elasticity vary strongly in space. The present results provide a novel view of the general interplay between membranes and proteins.

We acknowledge H. J. C. Berendsen for fruitful discussions. We thank the Finnish Cultural Foundation, Academy of Finland, Swedish Research Council, Foundation for Strategic Research, the Marie Curie research program, and the Netherlands Organisation for Scientific Research (NWO) for financial support.

[1] R. S. Cantor, J. Phys. Chem. B **101**, 1723 (1997).
[2] M. F. Brown, Chem. Phys. Lipids **73**, 159 (1994).
[3] A. V. Botelho *et al.*, Biophys. J. **91**, 4464 (2006).
[4] S. A. Safran, *Statistical Thermodynamics of Surfaces, Interfaces, and Membranes* (Addison-Wesley, Reading, MA, 1994).
[5] R. H. Templer *et al.*, Faraday Discuss. **111**, 41 (1999).
[6] T. Kamo *et al.*, J. Phys. Chem. B **110**, 24987 (2006).
[7] J. Sonne *et al.*, J. Chem. Phys. **122**, 124903 (2005).
[8] E. Lindahl and O. Edholm, J. Chem. Phys. **113**, 3882 (2000).
[9] J. Gullingsrud and K. Schulten, Biophys. J. **86**, 3496 (2004).
[10] S. Ollila *et al.*, J. Phys. Chem. B **111**, 3139 (2007).
[11] O. H. S. Ollila *et al.*, J. Struct. Biol. **159**, 311 (2007).
[12] P. S. Niemelä *et al.*, PLoS Comput. Biol. **3**, 304 (2007).
[13] J. Gullingsrud *et al.*, Mol. Simul. **32**, 831 (2006).
[14] S. Sukharev *et al.*, Nature (London) **409**, 720 (2001).
[15] S. Yefimov *et al.*, Biophys. J. **94**, 2994 (2008).
[16] P. Schofield and J. R. Henderson, Proc. R. Soc. A **379**, 231 (1982).
[17] R. Goetz and R. Lipowsky, J. Chem. Phys. **108**, 7397 (1998).
[18] J. H. Irving and J. G. Kirkwood, J. Chem. Phys. **18**, 817 (1950).
[19] See EPAPS Document No. E-PRLTAO-102-030909 for technical details. For more information on EPAPS, see http://www.aip.org/pubservs/epaps.html.
[20] J. S. Rowlinson and B. Widom, *Molecular Theory of Capillarity* (Clarendon Press, Oxford, 1982).
[21] G. B. Arfken and H. J. Weber, *Mathematical Methods for Physicists* (Academic Press, New York, 1995).
[22] H. J. Risselada *et al.*, J. Phys. Chem. B **112**, 7438 (2008).
[23] D. van der Spoel *et al.*, J. Comput. Chem. **26**, 1701 (2005).
[24] S. J. Marrink *et al.*, J. Phys. Chem. B **108**, 750 (2004).
[25] S. J. Marrink *et al.*, J. Phys. Chem. B **111**, 7812 (2007).
[26] L. Monticelli *et al.*, J. Chem. Theory Comput. **4**, 819 (2008).
[27] S. J. Marrink and A. E. Mark, J. Am. Chem. Soc. **125**, 15 233 (2003).
[28] P. Moe and P. Blount, Biochemistry **44**, 12 239 (2005).
[29] D. Marsh, Chem. Phys. Lipids **144**, 146 (2006).
[30] J. Jeon and G. A. Voth, Biophys. J. **94**, 3497 (2008).